Journal of Catalysis 308 (2013) 291–305

Contents lists available at ScienceDirect

Journal of Catalysis

journal homepage: www.elsevier.com/locate/jcat

In situ Transmission Electron Microscopy of catalyst sintering

Andrew T. DeLaRiva [a], Thomas W. Hansen [b], Sivakumar R. Challa [a], Abhaya K. Datye [a,*]

[a] University of New Mexico, Department of Chemical & Nuclear Engineering and Center for Microengineered Materials, MSC 01 1120, Albuquerque, NM 87131-0001, USA
[b] Center for Electron Nanoscopy, Technical University of Denmark, DK-2800 Kgs. Lyngby, Denmark

ARTICLE INFO

Article history:
Received 11 March 2013
Revised 20 July 2013
Accepted 18 August 2013
Available online 23 September 2013

Keywords:
In situ
Electron microscopy
ETEM
Sintering
Ostwald ripening
Particle migration
Coalescence
Nanoparticles
Monte Carlo simulation

ABSTRACT

Recent advancements in the field of electron microscopy, such as aberration correctors, have now been integrated into Environmental Transmission Electron Microscopes (TEMs), making it possible to study the behavior of supported metal catalysts under operating conditions at atomic resolution. Here, we focus on *in situ* electron microscopy studies of catalysts that shed light on the mechanistic aspects of catalyst sintering. Catalyst sintering is an important mechanism for activity loss, especially for catalysts that operate at elevated temperatures. Literature from the past decade is reviewed along with our recent *in situ* TEM studies on the sintering of $Ni/MgAl_2O_4$ catalysts. These results suggest that the rapid loss of catalyst activity in the earliest stages of catalyst sintering could result from Ostwald ripening rather than through particle migration and coalescence. The smallest particles are found to disappear in a few seconds as soon as the catalyst reaches the operating temperature. While particle migration and coalescence is evident in some of these *in situ* studies, it does not follow the classical model where the smallest particles are most mobile. Deterministic models of Ostwald ripening as well as atomistic Monte Carlo simulations are both in good agreement with these experimental observations, predicting a steep loss in catalyst activity at short times on stream. The *in situ* studies show the importance of direct observations to deduce mechanisms and show the important role played by the support and the gas atmosphere (especially the presence of H_2O) on the rates of catalyst sintering.

1. Introduction

Ernst Ruska invented the electron microscope in 1932 [1], and the first commercial instrument was developed by Siemens in 1939. Almost immediately, electron microscopy was used for the study of heterogeneous catalysts. Electron microscopy has continued to play an important role in the study of heterogeneous catalysts, and the insights provided through high-resolution imaging continue to help in the design of improved catalysts. Examples are the identification of active sites in $Cu/ZnO/Al_2O_3$ methanol synthesis catalysts [2]; the role of promoters in ammonia synthesis catalysts [3]; the role of corner and edge atoms in ammonia synthesis on Ru [4]; and the role of the phase transformations from the oxide to the iron carbide phase in Fe Fischer–Tropsch catalysts, which is linked inextricably to the central problem of catalyst attrition [5,6]. Since this review is intended for the 50th anniversary of this journal, it is an opportune time to look back at electron microscopy in heterogeneous catalysis. Indeed, the first volume of this journal contains a report on the use of the electron microscope to study particle sizes of Pd catalysts [7]. Since then, the application of electron microscopy in the study of catalysts has continued to grow and has been extensively reviewed in recent years in archival publications [8] as well as in this journal [9]. A recent issue of the journal ChemCatChem was devoted to this subject [10].

The applications of electron microscopy to catalysts continue to advance and a search in Scopus of the terms "electron microscopy" and "catalyst" brings up over 24,902 citations. In view of the broad scope of this technique, we restrict this review to one important application of electron microscopy, the study of catalysts under *in situ* conditions (in the presence of a gas atmosphere and elevated temperatures), and specifically to the study of catalyst sintering, since this represents an important cause of catalyst deactivation. The last review of *in situ* Transmission Electron Microscopy (TEM) of catalysts was in 2006 [11] and did not focus specifically on catalyst sintering. Improvements in the spatial and temporal resolution now allow *in situ* TEM to offer greater insights into catalyst behavior and shed light on the prevalent mechanism of catalyst sintering. A better understanding is needed to develop catalysts that are sinter resistant and self-regenerable. Fig. 1 shows a time-lapse image-series of a $Ni/MgAl_2O_4$ catalyst imaged in a TEM in an atmosphere of H_2/H_2O at 750 °C, from the doctoral thesis of DeLaRiva [12]. It shows the disappearance of small particles of Ni and the growth of larger ones. However, such a time-lapsed image sequence does not help us to deduce the mechanism, since the

* Corresponding author.
E-mail address: datye@unm.edu (A.K. Datye).

0021-9517/$ - see front matter © 2013 Elsevier Inc. All rights reserved.
http://dx.doi.org/10.1016/j.jcat.2013.08.018

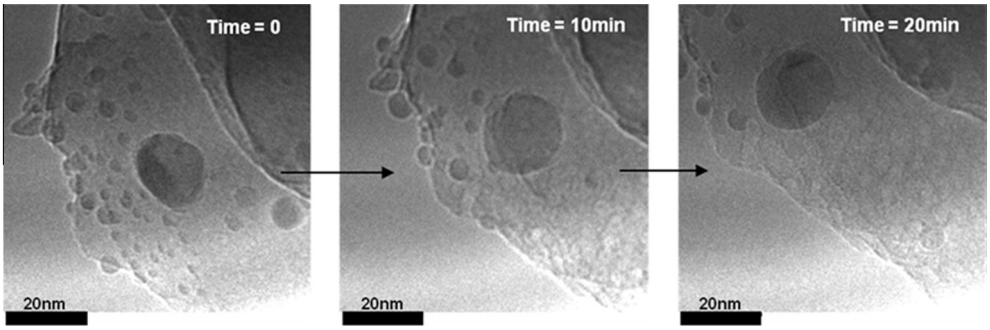

Fig. 1. A time-lapse series of images of $Ni/MgAl_2O_4$ from a movie recorded after *in situ* observation at 750 °C and a pressure of (1:1) H_2O:H_2 with total pressure of 3.6 mbar (adapted from DeLaRiva [12]).

nanoparticles could have grown due to migration and coalescence, or they could have coarsened through the process of Ostwald ripening, the two main mechanisms of nanoparticle sintering. Hence, we focus this review on *in situ* studies that help shed light on the mechanistic aspects of catalyst sintering and specifically to supported metal catalysts. Additionally, this review focuses on *in situ* studies published in the past decade.

We make references to the early work and to reviews that describe *in situ* TEM studies that originated through the work of Feates [13] at AERE Harwell in the UK and continued through the work of Baker [14]. Undoubtedly, the developments pioneered by Gai and Boyes [15,16] at Du Pont and then later by Hansen et al. [3] at Haldor Topsøe A/S played a pivotal role in the evolution of environmental TEM instruments, and modern versions of these designs are in use worldwide. We first review some of the instrumental developments, then describe results of recent studies, and then finally end with an overview of how modeling could help relate short term studies done via *in situ* TEM to long-term performance of industrial catalysts.

2. Environmental Transmission Electron Microscopy (ETEM)

Shortly after the invention of the electron microscope [1,17], exposing samples to a gaseous atmospheres in the millibar regime was also envisioned. Initially, this interest came from the biological sciences community, but later, the materials science community also got involved [18,19]. One of the main objectives was to study reduction and oxidation processes. From the beginning, the way to realize high pressures in the sample region of the microscope was by confining the gas with apertures around the sample region [18]. Swann et al. incorporated pressure limiting aperture systems, where the reactor was inserted into the electron microscope [20]. This method worked, but only low magnifications were possible. This concept was later refined by Hashimoto and coworkers in Japan [21] and by Baker and coworkers in the UK [22]. Both designs incorporated pressure limiting apertures as well as a resistive heating system. The main advantage of these systems was that they were microscope independent and could be moved between multiple facilities. Some decades later, this differential pumping system was built into the microscope column [15]. Such a design is independent of the stage design, and any microscope compatible holder could be used, facilitating different interactions with the specimen. This design was then used on an Environmental Transmission Electron Microscope (ETEM) with a field emission electron source, improving the information limit to 1.4 Å [3,11,23–26]. These instruments formed the later basis of the FEI Titan ETEM instrument widely used today [27–30].

In parallel with the development of the ETEM, gas injection holders and windowed holders have been developed. In these holders, the gas injection system supplies gas around the sample very locally and in very small amounts and much higher pressures can be attained without any supplementary pumping being needed [31,32]. The windowed-cell approach relies on electron transparent windows around the sample [33]. Using such a holder, pressures up to 4 bar have been demonstrated [34]. However, since a 200–300 kV electron beam can ionize gas, electron–gas interactions became significant [28,35]. Conducting ETEM experiments at elevated temperatures is always a challenging task. Most conventional heating holders are designed to operate in high vacuum, and the presence of an oxidizing agent can cause the heater to break down due to oxidation. Furthermore, the implementation of a heating filament in the holder takes up considerable space in an already highly spatially constrained environment. The bulkiness of these holders and the fact that the entire holder is heated imposes significant drift during heating, inherently limiting the spatial resolution. Despite these challenges, it is still possible to view nanoparticles of a catalyst in a heated environment under oxidizing or reducing conditions, and the movies we recorded for $Ni/MgAl_2O_4$ reported here were obtained with this conventional design. Recently, a new generation of heating holders has been commercialized. Using a Micro Electro Mechanical Systems (MEMS) approach, a window that is a few hundred microns across is used as a hot plate [36]. In a slightly different approach, Creemer and coworkers used a heater coil made from titanium nitride on a thinned silicon wafer [37]. Both approaches have the advantage of making possible a small area of uniform temperature and, therefore, very limited drift as the temperature is increased. However, accurate temperature measurement in these holders when a gas is passed over the sample still remains a challenge.

Baker and coworkers at AERE Harwell were among the most active in the development and use of ETEMs [22]. The work was later continued at Exxon. Baker et al. studied the formation of carbonaceous filaments formed during the decomposition of hydrocarbons on metallic nickel nanoparticles [22,38,39]. Later, the group moved on to study the mobility of nanoparticles in real time [39,40]. All these studies were conducted with a setup where the gas was confined around the sample by apertures built into the sample holder itself. The microscope resolution was limited in these early studies. With advancements in technology came increased resolution, sensitivity, and the faster image capture rate helped show the power of *in situ* TEM studies in clarifying the mechanisms of growth and the resulting morphology of carbon nanofibers [11,24]. This contribution focuses on recent work on the sintering of supported metal catalysts. The studies published over the past decade have been classified them into two groups, the first group where the authors concluded that nanoparticle mobility and coalescence was important while the second group where the primary observed mechanism was Ostwald ripening. The classification into two sets of studies helps the reader see conditions where particle

migration becomes important helping gain better insight into the contribution of this mechanism to catalyst sintering. Tables 1 and 2 provide a summary of these two sets of studies. Finally, we also include our results on $Ni/MgAl_2O_4$, followed by the use of mechanistic modeling to relate *in situ* studies to the operational performance of the industrial catalysts.

3. *In-situ* TEM of catalyst sintering

3.1. Particle Mobility leading to Coalescence

A list of *in situ* TEM studies identifying catalyst sintering by migration and coalescence is presented in Table 1. This table includes events that occurred directly by interaction with the electron beam and also with the environment and support. Coalescence events have been seen to occur quite rapidly; thus, it is imperative to have advanced microscope technology capable of capturing the events in real time. Chen et al. [41] report a study using high-resolution STEM coupled with an *in situ* thermal annealing stage of surfactant-free, monodispersed super-paramagnetic PtFe (cubic) alloy nanoparticles (~2 nm in diameter) stabilized in or on a KCl matrix. *Ex situ* experiments confirmed that annealing produces PtFe (tetragonal) ordered intermetallic nanoparticles with a mean diameter of 5 nm, and the *in situ* study revealed that the mechanism of nanoparticle growth is dominated by particle–particle coalescence, although Ostwald ripening is also implicated in a few regions. In addition, to determine the time dependent evolution of the size distribution of an ensemble of over 400 nanoparticles, analysis of the *in situ* data also allows tracking of individual nanoparticles, distinguishing coalescence from Ostwald ripening, nanoparticle by nanoparticle. There were very few Ostwald ripening events (4 incidences out of 150 particles) compared to coalescence events (22 incidences out of 150 particles) over 2 hours of annealing at 650 °C. However, since the melting point of KCl is 770 °C, it can be inferred that the observations were carried out at temperatures (600 °C) considerably above the Tammann temperature (~0.5 times the absolute bulk melting temperature), and it is possible that the observed phenomena could be influenced by the mobility of the support.

Yoshida et al. [42] used spherical-Aberration-Corrected Environmental Transmission Electron Microscopy (AC-ETEM) to study the catalytic activity of platinum on amorphous carbon electrode catalysts of proton-exchange-membrane fuel cells. These electrode catalysts were characterized under different atmospheres, such as hydrogen, air, and high vacuum (10^{-5} Pa). A high-speed charge coupled device camera was used to capture real-time movies to dynamically study the diffusion and reconstruction of nanoparticles with an information transfer down to 0.1 nm, a time resolution below 0.2 s. With such high spatial and temporal resolution, AC-ETEM permits the visualization of surface-atom behavior that dominates the coalescence and surface-reconstruction processes of the nanoparticles. The change in the specific surface area of platinum particles was evaluated in hydrogen and air atmospheres. Note that a primary electron energy of 300 keV, with an estimated

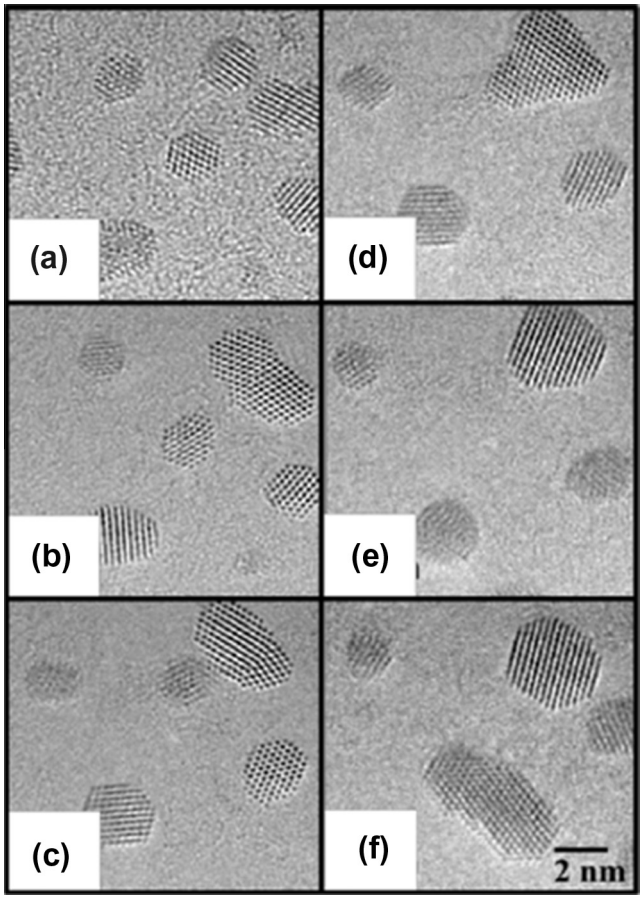

Fig. 2. Selected-area captured images obtained from a movie showing the coalescence process of Pt nanoparticles in 80 Pa of H_2 gas with times being (a)–(f) 0.00, 1.59, 5.32, 6.08, 7.01, and 8.34 seconds respectively (adapted from Yoshida et al. [42]). The sample was at ambient temperature, any heating would be caused by the electron beam.

Table 1
In Situ TEM Studies Showing Nanoparticle Mobility Leading To Coalescence.

Author	Metal/Support	Size	Temperature & Environment	Observations
Yoshida et al. 2013[42]	Pt/ Amorphous Carbon	2-3 nm	E-beam heating in vacuum (10^{-5} Pa), H_2, air (80 Pa)	CH_4 or CO_2 formation could be responsible for enhanced migration and coalescence
Chen et al. 2013 [41]	Pt-Fe/ KCl	2 nm → 5 nm	600 °C; Vacuum	Coalescence of Pt and Fe is observed, but note that the melting point of support is 770 °C
Aydin et al. 2012[44]	Ir/ MgO	Ir_1, Ir_4 clusters; 1 nm Ir	E-beam heating in vacuum	No coalescence despite particle contact for 1 nm particles. Otherwise mechanism is coalescence.
Janowska et al. 2011[43]	Pt, Pd/ Few Layer Graphene (FLG)	2-3 nm Pt	200-400 °C in vacuum	Coalescence of Pt nanoparticles at graphene edges.
Hansen PhD 2006[63]	Ni/ $MgAl_2O_4$	2-50 nm	750 °C; 4 mbar H_2/H_2O	Rapid coalescence of larger Ni particles after random migration
Liu et al. 2004[46]	Pd/ Al_2O_3 and carbon covered Al_2O_3	2-20 nm	300 °C – 700 °C; 500 mTorr H_2O	Carbon lifts the particle from alumina surface & gasification causes mobility
Ruckenstein & Lee. 1984[47]	Ni/ Carbon-Al_2O_3	5-15 nm	730 °C; H_2 and O_2	Rapid migration of Ni on carbon covered alumina due to gasification of carbon
Baker. 1979[14]	Pt/ Graphite single crystal	10 nm	750 °C; 5 Torr O_2	Mobility with channeling due to oxidation of carbon

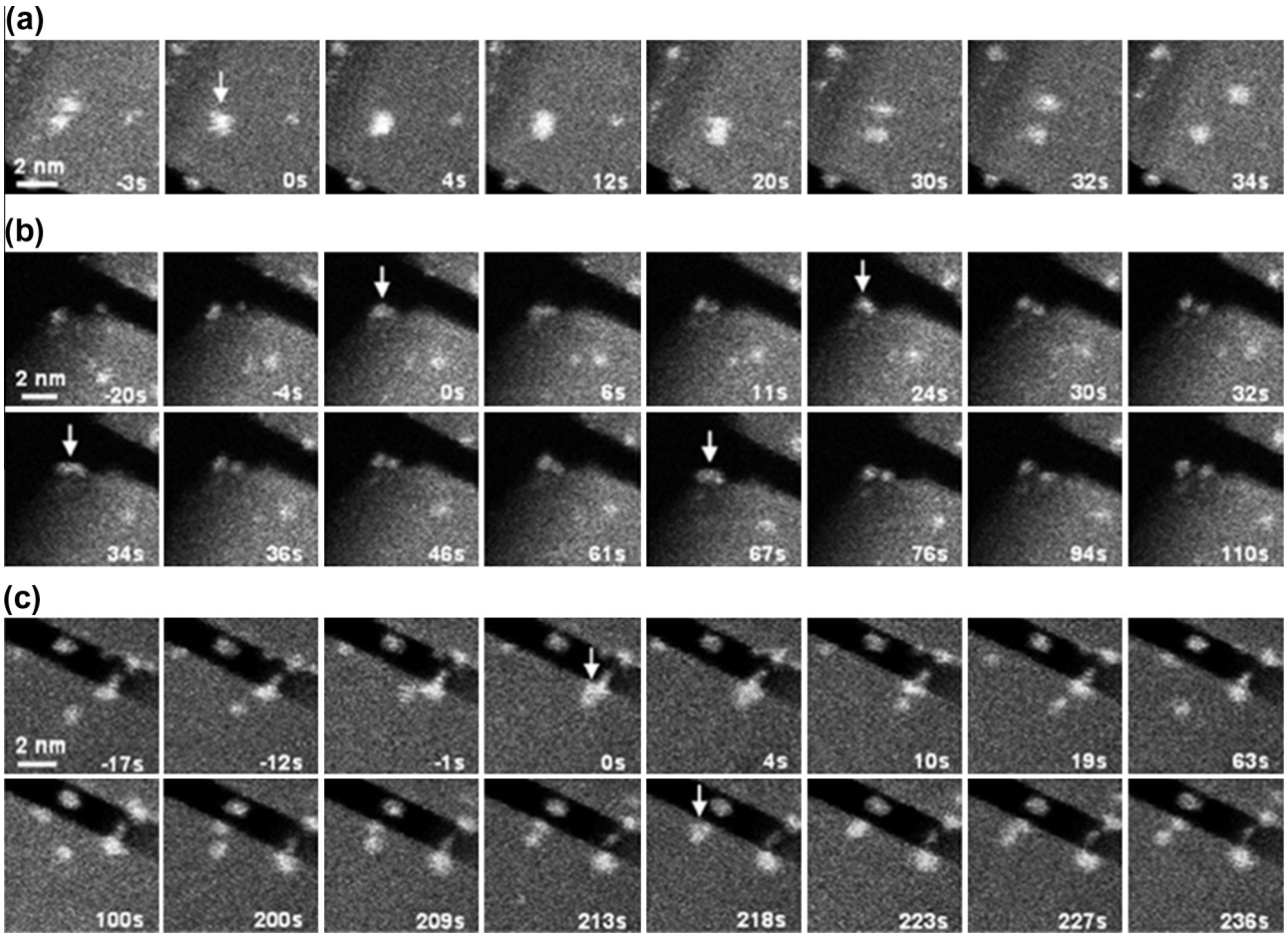

Fig. 3. Sequences of HAADF-STEM images showing lack of coalescence of iridium clusters with diameters of approximately 1 nm on MgO. (a) Collision of two clusters. (b) Multiple collisions of two clusters. (c) A cluster colliding with two clusters. The white arrows indicate the collisions, and the time for the first collision is set arbitrarily to be 0. The electron doses received by the sample during the imaging time were approximately $(10^5–10^6)e^-$ Å^{-2}, $(10^6–10^7)e^-$ Å^{-2}, and $(10^6–10^7)e^-$ Å^{-2} for sequences (a), (b), and (c) (adapted from Aydin et al. [44]).

current density of 178 A/cm^2, was used, which also acted as the mode of sample heating. The authors attribute the increase in atomic mobility to electron illumination and conclude that surface-atom diffusion dominates the crystal growth of Pt nanoparticles on amorphous carbon in high vacuum. Ostwald ripening leads to formation of well defined facets for the Pt nanoparticles. On the other hand, when the authors heated their samples in 80 Pa of H_2 or air, they observed that coalescence events dominated the process of Pt sintering (see Fig. 2). They found that carbon atoms were lost from the amorphous carbon (during electron beam exposure), possibly transformed into hydrocarbons (in H_2) or carbon dioxide (in air). The holes in the carbon film provided evidence of these chemical reactions. The removal of carbon would make the carbon rougher and thinner, leading to enhanced mobility of the Pt atoms on the carbon support. The decrease in the support surface area accelerates the coalescence of the Pt nanoparticles. The increased sintering rate in air was caused by the oxidation of amorphous carbon in air being faster than hydrocarbon formation in H_2.

Janowska et al. [43] report an *in situ* study of Pt nanoparticle sintering on few layer graphene (FLG) support. The particles were observed to be quite stable, and this was attributed to the strong interaction with the FLG. The reported images are at low magnification, making it difficult to infer the mechanism. However, locally, at the FLG edges, the Pt particles merge together, leading to a local buildup of cluster-like morphologies extending up to 10 nm. This happens in regions where the particle density is higher than on the smooth graphene surface. High-resolution TEM was used to obtain further insight into the microstructure of the Pt nanoparticles. The *in situ* thermal treatment induces local particle coalescence, leading to formation of clusters with dimensions up to 10 nm. It appears that the locally high concentrations of Pt lead to the observed coalescence of these particles.

In a study by Aydin et al. [44], the authors report that the primary sintering mechanism observed for Ir/MgO was particle migration and coalescence. However, they found that clusters around 1 nm in diameter were unusually stable and, even after collision, were found to separate, as shown in Fig. 3. The authors cite a DFT study that suggests the unusual stability of Ir to be a consequence of the formation of cube-shaped highly stable clusters. The authors propose this to be a general phenomenon that may have broad applicability. Furthermore, the authors state that "the evidence weighs strongly against the ripening mechanism in our experiments—because if there had been vapor-phase transport of Ir atoms, some of them very likely would have formed isolated species on the support." Ostwald ripening (OR) most likely involves emission of atoms (or mobile species) on the support (which is a lot easier than emitting atoms to the vapor phase, due to a lower energy barrier), and as shown in the next section, OR generally leads to larger average particle size. Only under special conditions, where isolated atoms can be trapped on the support (see the work of Hirata et al. [45] in the next section), would one expect to generate smaller particles during OR.

A study by Liu et al. [46] used *in situ* TEM to study the rapid sintering that happens during the regeneration of Pd/alumina catalysts used for acetylene hydrogenation. The authors found that sintering was very slow when the fresh catalyst was heated in steam. High temperatures, especially above the Tammann temperature (641 °C for Pd), were necessary for particle sintering to occur within a few hours. Both sintering mechanisms (ripening and coalescence) were observed in their experiments, but ripening was reported to be more influential as the used catalyst revealed that the Pd particles were essentially embedded in a hydrocarbon matrix. Catalytic gasification of hydrocarbon allowed the metal particles to move and coalesce with other particles, and sintering happened at a much lower temperature (~350 °C) during the oxidation process and, even, within 1 h. It is possible that the local temperature around the Pd particles during hydrocarbon oxidation was considerably higher than the readout temperature of 350 °C. However, the increase in particle mobility and the occurrence of coalescence events was related to the gasification of the carbon which, the authors report, "lifted" the particles from the alumina support which were essentially embedded in a hydrocarbon matrix.

A similar high mobility of metal nanoparticles was reported in the work of Ruckenstein and Lee who studied Ni particles deposited on alumina covered by carbon [47]. Movement of the metal particles left behind tracks on the support. The rapid movement could then be a consequence related to the gasification of carbon during the experiments. In light of the studies reported earlier in this section, where the mobility of nanoparticles was related to the reaction of the carbon support with the gas phase, it is entirely possible that a similar mechanism was operative.

Continuous observation of particle evolution in catalysts via controlled atmosphere electron microscopy was first reported by Baker and coworkers, who demonstrated that observations on a supported platinum catalyst at elevated temperatures were possible [39,40]. On oxide supports, these authors found that the Pt particles were immobile, and the authors speculated that all growth occurred due to the migration of particles smaller than 2.5 nm, which was the microscope resolution at that time. On graphite supports, the authors found that particles were mobile in the presence of CO and the mobility decreased with increasing particle size. Although the observations showed random migration of nanoparticles, the time resolution (recording intervals of one second) did not reveal what was happening to smaller particles (either due to the microscope point resolution or because the movies were recorded at a point in time when most of the small particles had disappeared).

There is a real question as to the mechanisms that cause mobility of nanoparticles. Since these observations are all performed in the presence of an electron beam, and as some aforementioned studies relied on electron beam heating which does not provide any measurement of local temperature, one should consider forces that could arise due to the perturbation of the metal particles by the electron beam. Recent work by Batson et al. [48,49] shows that attractive forces can arise due to the presence of the electron beam, causing particles to move on the surface. However, when the particles approach each other, there may be a barrier preventing coalescence. The final process then can involve the formation of a "bridge" between the nanoparticles and the ultimate disappearance of the small particle via Ostwald ripening. Fig. 4 shows how migration and coalescence can be caused by an aloof electron beam, but in the end, the disappearance of the particle is aided by Ostwald ripening [48]. We have observed similar behavior in the case of Pd/carbon where particles in close proximity formed a neck leading eventually to the disappearance of the small particles [50]. An alternate explanation has been proposed for the observed coalescence and has been termed attractive migration and coalescence [51]. Attractive migration and coalescence has been seen to operate when the nanoparticles are separated by as much as 4.5 times the radius of the islands, even ~300 nm. And while the mechanism is termed coalescence, the underlying phenomena involve the motion of atoms, essentially Ostwald ripening. It is therefore clear that ripening can be responsible even for the neck formation seen when two particles are in close proximity.

3.2. Ostwald Ripening

A summary of recent *in situ* TEM studies of catalyst sintering by Ostwald ripening is presented in Table 2. The major improvement in image resolution through the correction of spherical aberrations makes it possible to resolve isolated single atoms, especially on carbon supports. Since Ostwald ripening involves the migration of atomically dispersed species, it is of interest to see what we

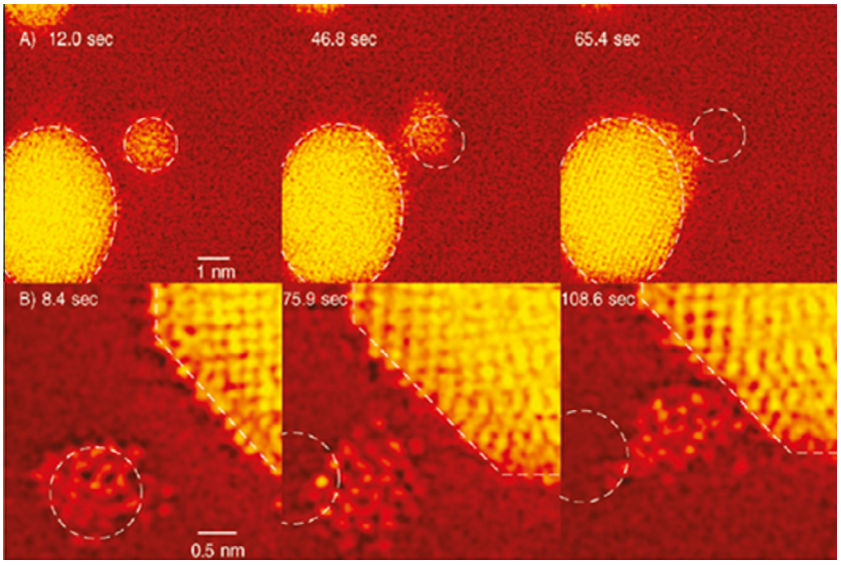

Fig. 4. Beam induced coalescence of two smaller Au particles (A) and (B) with larger Au particles. The authors caused the beam to stop at different locations relative to the particles. They conclude that the polarization caused by the transmitted electrons results in these coalescence events (adapted from Batson et al. [48]).

Table 2
In Situ TEM Studies Showing Ripening Of Nanoparticles.

Author/Year	Metal/Support	Size	Temperature & Environment	Observations
Yoshida et al. 2012[52]	Pt/ Amorphous Carbon	1.6-2 nm	E-beam heating in vacuum	Numerous observations of mobility of single Pt atoms mobility leading to Pt ripening
Hansen et al. 2012[29]	Au/Graphene	2-5 nm	RT, 100 °C, 400 °C; vacuum or 200 Pa H_2	Ripening was observed and also coalescence of neighboring particles. Restructuring of graphene under e-beam was detected.
Hirata et al. 2011[45]	Pt/CeO_2	2-7 nm	750 °C; vacuum and 1 Pa O_2	Redispersion of metal via mobile Pt-oxide species. Pt size decreases in O_2 and regains its size in vacuum, without any noticeable movement.
Simonsen et al. 2010[65]	Pt/Alumina, Pt/SiO_2	~3 nm,	650 °C in 10 mbar air	Pt ripening (probably via Pt-oxide mobility), local correlations influence ripening rates
Hansen et al. 2010[27]	Au/Boron-Nitride	2-4 nm	400 °C; 130 Pa H_2	Ripening of smaller particles. Possible rapid migration of particles and subsequent coalescence.
Kim et al. 2010[58]	Fe/Al_2O_3	4 nm	650 °C; 2.5 mTorr C_2H_2 + 7.5 mTorr H_2O	Ripening of Fe particle growing a SWCNT. Surface ripening on Al_2O_3 in the initial 5 minutes, followed by subsurface diffusion. Likely mobility of particles on a carbonaceous coating.
DeLaRiva PhD 2010[12]	Ni/$MgAl_2O_4$	2-25 nm	750 °C; 3.6 mbar H_2/H_2O	Ripening of small Ni particles at very early stages of heating. Size decay/growth profiles resemble ripening.
Amama et al. 2009[57]	Fe/Al_2O_3	6-10 nm	650 °C; H_2/H_2O	Ripening: based on growth of particles catalyzing nanowires. Ripening inhibited in H_2O.
Creemer et al. 2008[33]	Cu/ZnO	0 → 5-10 nm	RT- 500 °C; 1.2 bar H_2	Appearance of Cu particles from reduction of CuO, with growth indicative of ripening. Transient migration or mostly immobile particles
Hannon et al. 2006[54]	Au on top of Si nanowires	50-80 nm	655 °C; 0.5 mTorr $(SiH_3)_2$	Ripening leads to change in Au island size which affects nanowire diameter. Mobile Au species travel from one wire to another

can learn by application of the newest microscopes for the study of catalyst sintering.

Fig. 5 shows images obtained using aberration corrected TEM by Yoshida et al. [52]. The images show the presence of single atoms of Pt on amorphous carbon films and their movement, indicating the process of Ostwald ripening. A high beam current (40–60 A/cm^2), along with a high energy of irradiation (300 keV), acted as an indirect mode of heating for the supported metal catalyst. The time resolution (1 frame per second) was inadequate to note the rapid motion of these single atoms on the support, but a net change in the number of atomic columns was noted over time in two neighboring particles, from which ripening was deduced to be the main mechanism. The high-resolution imaging clearly showed local correlations during the ripening of these two particles. These two neighboring particles were nearly of the same size initially; however, the shrinking particle happened to be abutted by a hole in the supporting amorphous carbon film, plausibly lowering its stability and, consequently, causing it to lose its constituent atoms over time. It is remarkable to be able to capture such dynamic transient processes and to shed light on the importance of heterogeneities in sintering of supported nanoparticles. This *in situ* study also identified the possibility of bi-atoms or few-atom clusters mediating the ripening, though a more quantitative study would be needed to ascertain their relative roles in the overall ripening rates. We add, however, a note of caution about interpreting phenomena that occur due to electron beam irradiation, since they may not follow the same mechanism as in a catalytic reaction that is thermally activated. We feel it is necessary to perform *in situ* studies where heating of the sample is controlled, causing the observed changes in catalyst morphology, as it is in real-world catalysts.

The work of Hansen and Wagner [29] is a recent study where an aberration corrected TEM was used to study the evolution of Au on graphene. At room temperature, the authors reported that, in the

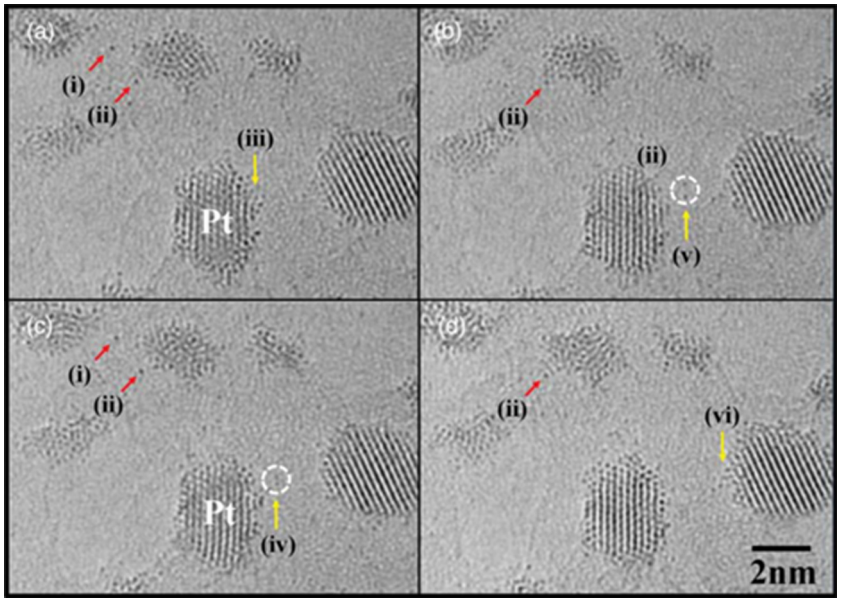

Fig. 5. Set of images obtained from an *in situ* video revealing the beam induced movement of individual Pt atoms on an amorphous carbon film (adapted from Yoshida et al. [52]).

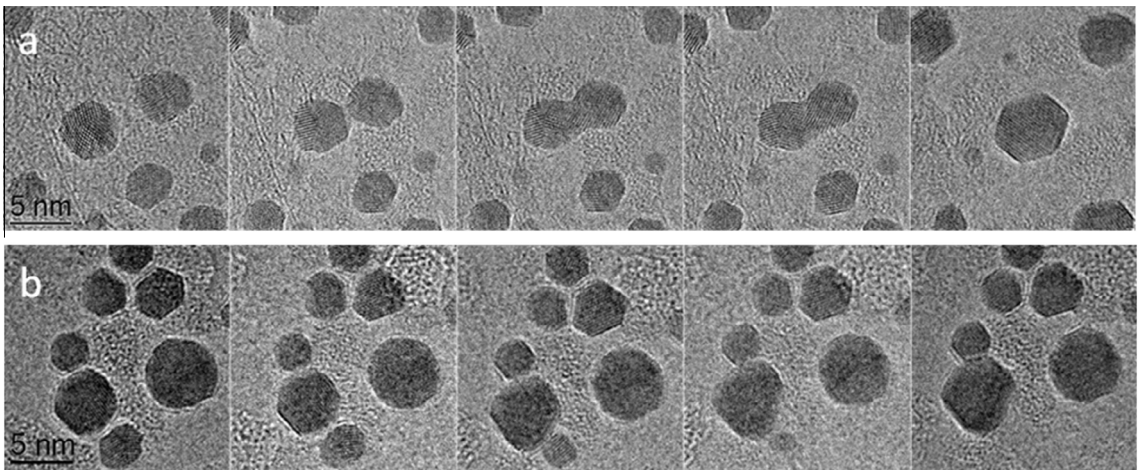

Fig. 6. (a) Set of images taken from a movie showing Au on graphene revealing the coalescence of adjacent particles in 200 Pa H_2 at 100 °C. The images were taken at 0, 55, 56, 58, and 94 seconds. (b) The ripening of a Au particle (lower left in images) at 400 °C in 200 Pa H_2. The image set was taken at 0, 13, 42, 46, and 48 seconds. The graphene support is also seen to change structure over time (adapted from T. Hansen and J. Wagner [29]).

presence of the electron beam, the Au particles tend to make irregular movements around a fixed site rather than migrate laterally across the substrate, both in vacuum and in the presence of hydrogen. As the primary energy of the electrons is significantly above the threshold for knock-on damage of graphene sheets, such motion may be related to restructuring of the graphene substrate rather than be inherently related to the dynamics of the gold nanoparticles. Substrate restructuring is also observed in lower magnification image sequences where the graphene sheets, as a whole, change shape and deteriorate in the presence of the electron beam. Such restructuring can move the gold nanoparticles into direct contact with each other, subsequently resulting in particle coalescence. Even though the influence of the high-energy electrons on the graphene is significantly more pronounced at 300 keV compared to, for example, 80 keV, 300 keV was chosen due to the improved image resolution. Upon increasing the temperature, the gold nanoparticles became dynamic. When keeping the beam current density reasonably low, observation of coalescence events could be noted without significant damage to the supporting substrate. In most cases, the gold nanoparticles migrate as crystalline entities across the substrate. As they come into contact, a bridge of material is formed linking the particles together (see Fig. 6a). Once the bridge has been formed and atoms can migrate from particle to particle, an equilibrium state is quickly attained. The lattice fringes of both the constituent particles and the resulting particle are resolved throughout the process.

In Fig. 6b, stills extracted from an image sequence recorded at 400 °C in 200 Pa of hydrogen are shown. The lower particle in the images is seen to gradually become smaller, and the larger particle located just above it becomes larger, indicating a transfer of mass from the smaller to the larger particle. This shows that the particles under these conditions can grow by Ostwald ripening. Under the same conditions, rapid coalescence was also observed. The authors conclude that a single growth mechanism cannot be assumed. and presumably, the overall coarsening of the nanoparticle ensemble follows multiple routes. However, the mobility of the graphene substrates and the influence of the electron beam must be considered. Hence, it is instructive to review next some results on more industrially relevant oxide supports.

Hirata et al. [45] describe how *in situ* TEM could be used to also study the process of catalyst redispersion. This study was performed on Pt/Ceria–Zirconia–Yttria, and the authors found that the sintering of Pt occurring at 750 °C in vacuum could be reversed by adding O_2 at 1 Pa also at 750 °C. The particle size decreased considerably. Repeated switching of the gas environment from vacuum to O_2 environment gave rise to a reversible behavior in sintering and redispersion of Pt. Under O_2 conditions, a volatile Pt oxide species can be formed that is also highly mobile (Pt^{2+} or Pt^{4+}). The size of the nanoparticle decreases through emission of these species. Additional analyses indicate that the redispersion takes place via the mobile species getting trapped at sites on the support as Pt–O–Ce due to strong Pt–Ceria interaction. The redispersion phenomena were also studied using *in situ* EXAFS which revealed that Pt was in fact dispersed and highly oxidized on the support surface over the entire sample. This study clearly shows that the changes in the catalyst during redispersion were driven by mobile atomically dispersed species, *i.e.*, Ostwald ripening. The authors did not report any particle migration, and their *in situ* characterization also reveals that the location of the particle remains unchanged during the entire period that it is undergoing repeated reversible size changes in the process of sintering and redispersion.

In situ electron microscopy approaches have also been used to study the process of coarsening and Ostwald ripening in the context of growth of nanowires and nanofibers. Through a combination of ultra-high vacuum TEM (UHV-TEM) and low energy electron microscopy (LEEM), it was shown that the termination of silicon nanowire growth results from Ostwald ripening of the Au catalysts that mediate the vapor–liquid–solid growth process (Fig. 7) [53]. As shown in this figure, some nanowires stop growing because they have completely lost the Au catalyst at the tip, while others continue to grow. The nanowire is seen to grow (as well as diminish) in diameter too, corresponding to the size of the catalyst particle. As shown in the schematic diagram, the Au atoms have to travel down one nanowire and rise up another, indicating that these atomic species are quite mobile at the growth temperature of 655 °C. This ripening process was shown to be highly sensitive to the surface condition, occurring rapidly on clean Au-terminated Si surfaces while slowing down substantially in the presence of an oxygen-terminated surface [54,55]. Similar effects have been observed during the nucleation and growth of carbon nanotubes, through the use of Environmental Transmission Electron Microscopy [56–59]. Fig. 8 shows the influence of treatment conditions on the evolution of Fe catalyst particles that serve as catalyst for nanotube growth. Again, the surface condition and presence of small amounts of residual gas in the gas stream have been shown to have strong control over both the mechanism and rate, and small amounts of water vapor seem to slow down the rate of Fe

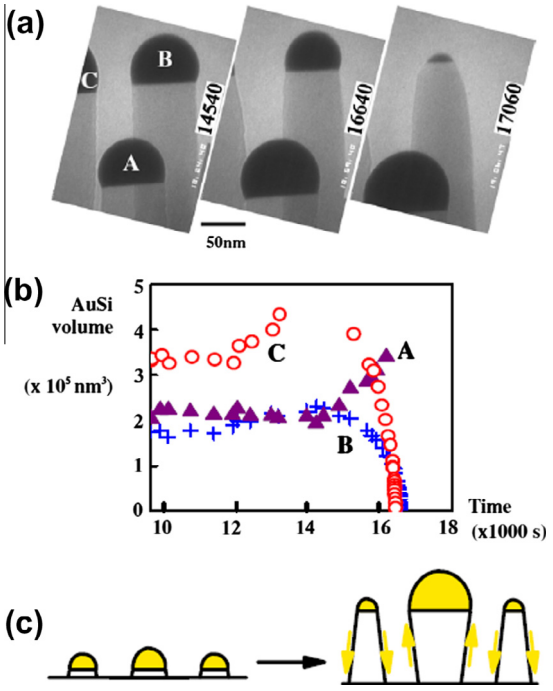

Fig. 7. Ostwald ripening of Au seen via *In situ* UHVTEM images recorded during the growth of Si nanowires at 655 °C in 10^{-6} Torr of disilane. (a) Three images labeled by the time (in seconds) after the start of growth. Scale bar: 50 nm. (b), Measured volume versus time for the catalyst droplets labeled in (a). (c) Schematic of how the Au atoms are transported during the nanowire growth (adapted from Ross [53]).

particle growth. The presence of small amounts of water vapor in the reactive gas stream was shown to dramatically improve the nanotube growth [60,61], and it has been shown that the primary role of water vapor is to inhibit the process of catalyst coarsening (Fig. 8), thereby increasing the time that nanotube growth occurs. Further studies have shown the importance of water vapor and substrate condition [60], as well as subtle effects due to interaction between water vapor and carrier gas, on the rates of nanoparticle ripening [61]. The effect of hydroxyl groups enhancing the stability of Au nanoparticles has also been reported in the literature [62].

Studies reviewed so far indicate that nanoparticle mobility can be observed on carbon supports, and we wanted to investigate this sintering behavior using Pd nanoparticles deposited on a thin carbon film. Fig. 9 shows the evolution of Pd nanoparticles that were generated in solution from the reduction of Pd-acetate. The primary phenomenon observed at 500 °C was Ostwald ripening, with some particles growing in size and others shrinking and disappearing completely [50]. Mobility or migration of the Pd nanoparticles was not observed at any time. Anomalous growth patterns where some particles continued to grow in size and become much larger than would be predicted based on a log-normal distribution were observed. These anomalous growth patterns can be seen experimentally but not accounted for theoretically. Such particles were also seen in the work of Amama et al. [57] (see Fig. 7).

Detailed quantitative analysis of changes in particle size facilitated by *in situ* studies has also enabled identification of other mechanisms of sintering that have hitherto been neglected in the mechanistic analyses. Yang et al. [51] have identified a combined ripening and coalescence mode that they term as attractive migration sintering. Based on observations of neighboring islands, it was shown that non-uniform concentration gradients around these islands propel them toward each other. We have observed similar events during *in situ* heating of Pd nanoparticles supported on carbon (under H_2 at 500–600 °C, see Fig. 9) [50] and can also be seen in the neck formation between the Au islands in the work of Hansen and Wagner [29] (see Fig. 6). It is clear that these anomalous growth patterns can be seen during conditions where

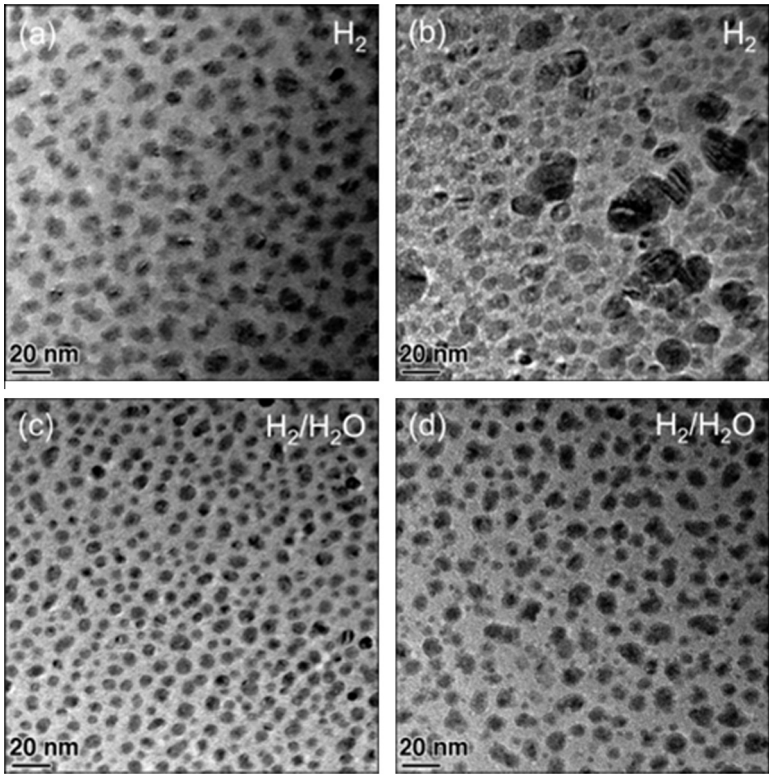

Fig. 8. TEM images of Fe catalyst nanoarticles in H_2 after (a) 30 s and (b) 5 min, and in H_2/H_2O after (c) 30 s and after (d) 5 min (adapted from Amama et al. [57]). The presence of H_2O significantly slows the rate of Fe sintering.

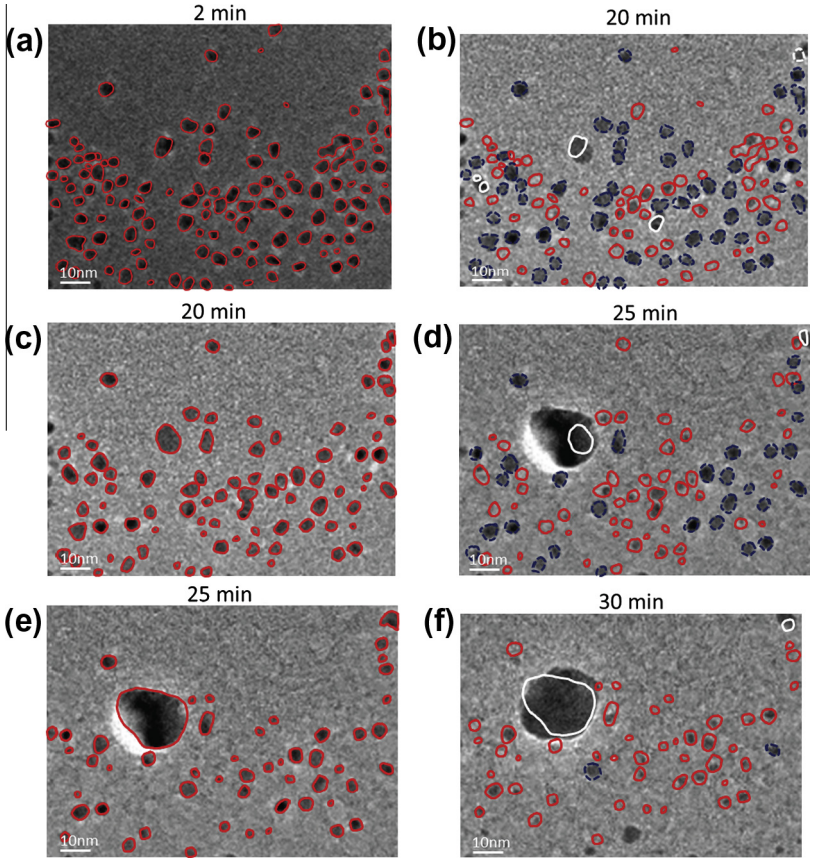

Fig. 9. The evolution of Pd particles on carbon in vacuum after heating to 500 °C at various times. Each image pair (a) goes to (b), (c) goes to (d), and (e) goes to (f) shows the sample before and after heating with corresponding particles outlined in color. The red particles have shrunk or disappeared, white particles have grown in size, and blue particles have remained the same (adapted from Benavidez et al. [50]). (For interpretation of the references to color in this figure legend, the reader is referred to the web version of this article.)

Ostwald ripening is the prevailing mechanism. Besides local correlation effects which lead to non-uniform concentrations on the support, the role of support structure and chemistry in mediating sintering needs to be analyzed and included in modeling to better predict the catalytic behavior of nanoparticle systems. A review of the literature in Table 2 summarizes experiments where Ostwald Ripening was the main mechanism of particle growth on oxide supports based on observed *in situ* studies for their specific system. Particle migration and coalescence is also seen on oxide supports, as shown in the work of Aydin et al. [44] in Fig. 3 and also in the work of Hansen [63] described in the next section in the study of Ni catalysts.

3.3. Spanning a time frame of seconds to hours

Most *in situ* TEM studies are conducted over short time durations due to experimental difficulties in maintaining steady-state operation in the presence of a gas atmosphere at elevated temperatures. It is not generally possible to leave a microscope unattended for long-term studies as is often done with chemical reactors. Hence, there are very few reported studies that span a long time frame with the same catalyst. Furthermore, most studies are performed on model catalysts to make it easier to study the phenomena occurring on the catalyst. Here, we report the results from the doctoral research of Hansen [63] and DeLaRiva [12] who performed a comprehensive series of experiments on Ni/$MgAl_2O_4$ catalysts (1 wt% and 12 wt% Ni) that were performed under conditions relevant to steam reforming of methane. The experimental details have been published elsewhere [12,63], so only a brief summary of the experimental conditions is provided in Supporting information. A 12 wt% Ni/$MgAl_2O_4$ catalyst that was reduced in the microscope at 500 °C before subjecting it to aging at temperatures ranging from 650 °C to 750 °C (ramping at ~50 °C/min) was used. In these experiments, the sintering of the Ni catalyst was captured within the first few seconds after reaching the operating temperature, and aging was continued for up to 10 h while maintaining the same gaseous environment and temperature in the microscope.

Fig. 1 in the Introduction presented a time-lapse sequence documenting the disappearance of nickel particles <3 nm under 360 Pa 1:1 H_2:H_2O at 750 °C with the electron beam switched off after each set of images was acquired. Disappearance of small Ni particles was seen consistently in multiple experiments of the early stages of heating, within the first 30 min after reaching the aging temperature of 750 °C. In each case, the beam was switched off between observations in order to first establish the phenomenon of sintering without the effects induced by the electron beam. The beam-off experiments provide information on the overall phenomenon at early times, which is a loss of small particles, but the mechanistic insights are only obtained from image sequences recorded at high temporal resolution immediately after reaching the operating temperature. The experiments of the early stages of heating were repeated with continuous observations of the sample. These real-time observations allowed investigations of the dynamics of Ostwald ripening during the earliest stages of catalyst sintering.

It is important to note here that the disappearance of individual particles during the initial stages of catalyst sintering can only be

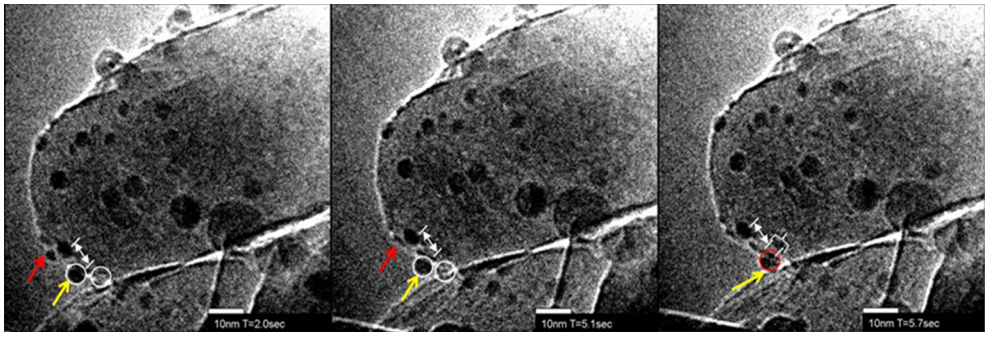

Fig. 10. Images taken from a movie sequence of a 12 wt% Ni/$MgAl_2O_4$ at 750 °C. The particle (~2.5 nm) indicated by the red arrow (left) is seen to ripen and disappear in the first pair of images, while the larger arrowed particle (~5 nm) shown with the yellow arrow migrated over the surface a distance equal to its own diameter and coalesced with a neighboring particle, which is not visible in the image and hence its location is shown by the white circle. The movie (in the supporting information, movie 1) shows this second particle and the coalescence event much more clearly. The double arrows show the initial separation of two particles, and the third image shows the increase in interparticle separation after the coalescence event (adapted from DeLaRiva [12]). (For interpretation of the references to color in this figure legend, the reader is referred to the web version of this article.)

seen if movies can be recorded at high magnifications and immediately after the elevated temperature is reached. If one waits till the sample stops drifting, the smallest particles may have already disappeared. It is well known that when a TEM sample is heated, there is considerable sample drift, as the sample holder equilibrates to the new temperature. Therefore, a method for allowing image capture as soon as the operating temperature was reached was developed (see Supporting information for more details). The images reported here were recorded at 100 ms/image as soon as a temperature of 750 °C was reached. A movie based on these images is included in the Supporting information, and still images from this image sequence are shown in Fig. 10. The image sequences recorded within the first few minutes of observation showed very few occurrences of particle migration and coalescence. One such migration event is highlighted in Fig. 10, where the particle moved and coalesced with a neighboring particle.

Ostwald ripening is characterized by the shrinking and disappearance of small particles with the mass being transferred to larger particles in the vicinity. In Fig. 10, the shrinkage and disappearance of a ~2.5-nm particle indicated by the red arrow is clearly seen; in these experiments, it is difficult to detect the growth of the larger particles, since the increase in diameter of the larger particles is imperceptible over short time intervals. However, the lower magnification beam-off experiments confirmed that mass was conserved within a given region; and the loss of Ni was not due to evaporation, which is much slower at these temperatures (see next section for further analysis of the disappearance of an individual nanoparticle [64]). It is also evident that not all particles disappear at the same rate. The particles which are seen to ripen away are close to the small critical size where changes can be observed. Additional factors could contribute to the different rates of ripening including the number and sizes of neighboring particles, faceting of individual particles and other changes in support morphology or texture that could not be detected at the resolution available in this microscope.

Fig. 11 shows a set of images from another experiment of the early stages of heating with continuous observations. Here, multiple instances of the disappearance of particles over the course of the four frames are observed. To capture the disappearance in real time, rapid acquisition is needed since these Ni particles ripen very quickly, usually within seconds. (The movie corresponding to this experiment can be found in Supporting information) We have extracted individual frames from an image sequence, a frame every 100 ms (10 fps), to show the disappearance of five of the particles. The particle size versus time plots for each of the labeled nanoparticles in Fig. 11 are shown in Fig. 12, and it is clear that the lifetimes of particles smaller than 2.5 nm are on the order of seconds. It is significant that the Ni particles are immobile and do not show any migration or coalescence. Fig. 12 also shows that the rate of change in particle diameter is very slow until the particle reaches a critical size, after which the entire event of disappearance is over in seconds. This trend was seen on multiple samples, in numerous areas on the support, and with varying beam intensities. These phenomena were only seen when the catalyst was heated to the operating temperature, and none of these events occurred simply due to beam exposure.

To determine whether the Ni ripening events could be caused by the beam, a comparison was made to recent work on Pt/Al_2O_3 catalysts, where careful measurements were performed with varying beam intensities to study the ripening of Pt under oxidizing conditions [65]. Under these conditions, a volatile Pt oxide can be formed that would lead to a decrease in size of the metal particles. The authors observed an almost linear dependence of the rate of decrease in mean particle diameter of a collection of Pt particles for beam current densities up to 1.0 A/cm^2 [65]. The electron beam intensities used for the present Ni/$MgAl_2O_4$ study varied with magnification, with the maximum beam intensity calculated to be 1.2 A/cm^2 (at a magnification of 270 KX and 7.4×10^4 electrons/nm^2 s). Most of the ripening events that were captured at this high dose rate in the present study lasted no more than 10 s (which is the time for the disappearance of the particles shown in Figs. 4 and 5).

Based on the work of Simonsen et al. [65], at the beam intensity used in the present experiments (1.2 A/cm^2), a decrease in mean diameter, of 0.137 nm/min, is expected. Thus, over an exposure period of 10 s, the apparent shrinkage of a Ni particle of size 2.5–3 nm (the particles most observed to ripen herein) due to electron beam exposure would be 0.025 nm, which is below the detection limit under these conditions. Furthermore, the experimental conditions used in these two studies are very different. For Pt under oxidizing conditions, the formation of a volatile Pt oxide is expected. For Ni under reducing conditions, the only volatile species expected is Ni metal atoms. An estimate of the rate of evaporation of Ni shows that it would take hours for a Ni particle of 2.5 nm to evaporate under our experimental conditions [64].

Since ripening was observed in beam-off experiments as well as experiments at lower magnifications (which have much lower beam doses ~0.4 A/cm^2), we are confident that artifacts caused by electron beam exposure in the Ni/$MgAl_2O_4$ study can be ignored. The rapid disappearance of small Ni particles during

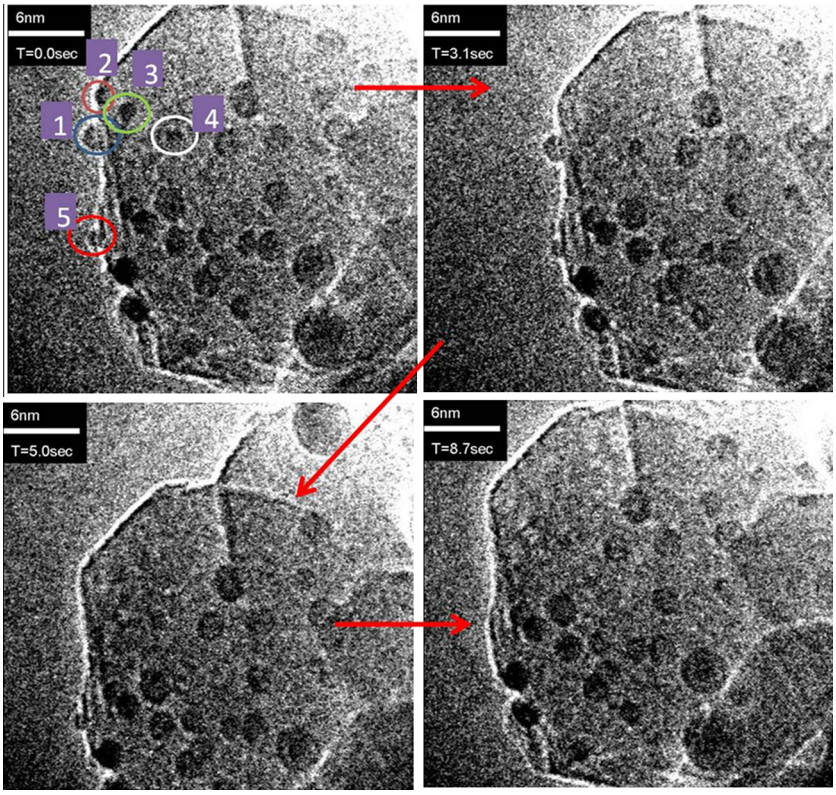

Fig. 11. Higher magnification movie of a ripening Ni particles in the 12 wt% $Ni/MgAl_2O_4$ in (1:1) $H_2O:H_2$ 3.6 mbar at 750 °C. Total elapsed time is 5.7 seconds (adapted from DeLaRiva [12]). The particles labeled 1–5 progressively disappear due to Ostwald ripening.

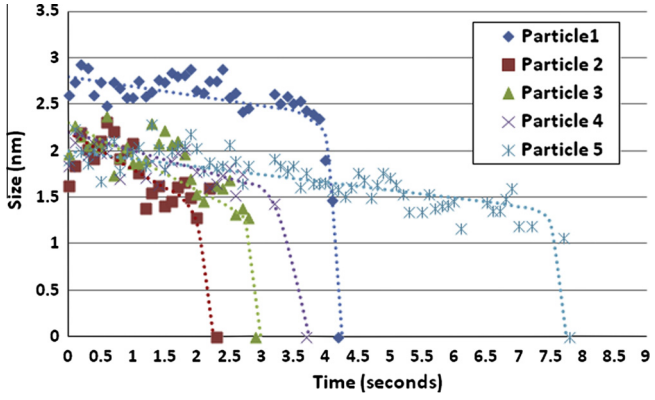

Fig. 12. Size vs. time for Ni particles from Fig. 11 undergoing ripening in 3.6 mbar $H_2O:H_2$ 1:1 at 750 °C. The dotted line shows a trend line describing the evolution of particle size with time (adapted from DeLaRiva [12]).

ripening is consistent with Monte Carlo simulations of the ripening of individual particles as described later. The effect of beam dose on the rates of particle migration and coalescence was also investigated, and it was found that the particle migration and coalescence events were only seen at elevated temperatures and could not be induced at room temperature simply by increasing the beam dose for this sample [63].

A second series of experiments was performed with a 1 wt% $Ni/MgAl_2O_4$ catalyst under conditions where the sample had thermally equilibrated and thermal drift was negligible. At this stage, most of the small particles had disappeared, and very little change could be seen in particle size over small intervals of operation time. Numerous such experiments were conducted [63]; in some cases, the sample was heated up to 10 h at the operating temperature. The major noticeable feature was occasional migration of individual particles that sometimes led to coalescence, but no ripening. An image sequence showing this phenomenon from a movie captured after about 60 min at 750 °C is shown in Fig. 13 (this movie can be found in Supporting information). The sample was heated in a 1:1 mixture of H_2 and H_2O at a total pressure of 4 mbar and 750 °C, and several migration and coalescence events have been noted. Migration of the nanoparticles was observed to be slow and random, but when the particles approached each other, coalescence happened very quickly, usually within one frame, *i.e.*, 1 s. Due to the rapid coalescence, no dumbbell shaped particles were seen in any of the images recorded at this high temperature. After acquisition, the frames were aligned using the statistically determined spatial drift (SDSD) analyzer for DigitalMicrograph by B. Schaffer et al. [66]. The success of this operation can be seen from the position of the sample edge at the lower corners of each frame. The image sequence shows both particle migration and coalescence. Such observations could indicate a gradual change from Ostwald ripening in the initial stages of catalyst sintering to a particle migration and coalescence mechanism during steady-state operation. However, with these *in situ* experiments, it was not possible to assess the contribution of the particle migration and coalescence events to the rate of catalyst sintering because these events were observed to be very random and difficult to capture.

The experiments performed on $Ni/MgAl_2O_4$ revealed the importance of *in situ* TEM as the experimental observations differed greatly from initial theoretical predictions for this system. Instead of observing highly mobile nanoparticles at the early stages of sintering, ripening of these particles was seen with an eventual change in mechanism over time. The experiments also revealed that a combination of sintering mechanisms, ripening and migration leading to coalescence, can both contribute and be equally responsible for the large loss in surface area. In addition, future work using higher pressures and additional gases could be performed in order to determine the effect on particle sintering for this system.

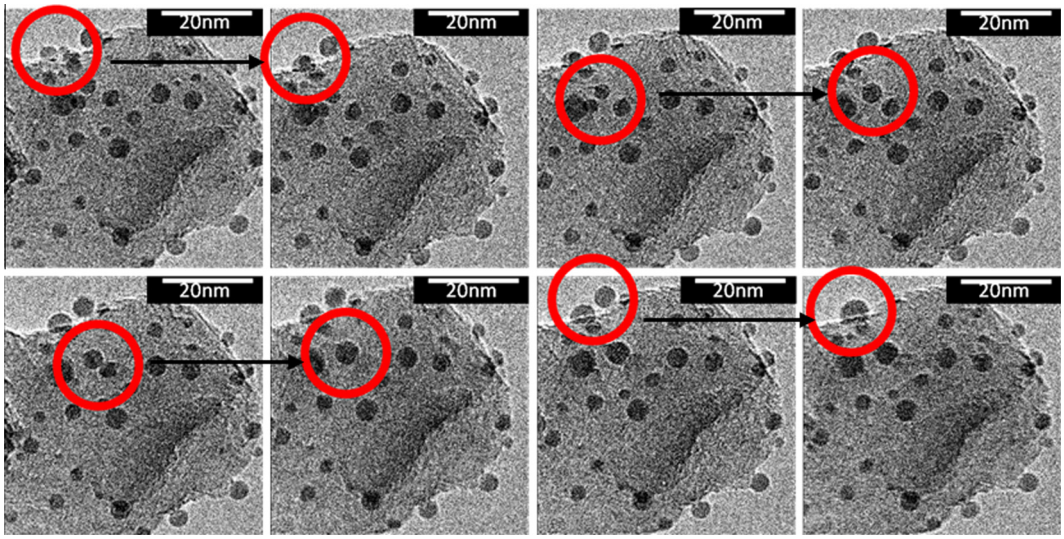

Fig. 13. Several Ni particle migration and coalescence events are seen on the surface of a 1 wt% Ni/$MgAl_2O_4$ under 4 mbar H_2O:H_2 1:1 at 750 °C (adapted from Hansen [63]) This movie was obtained after the sample had stabilized at temperature, hence there is minimal drift in the movie (see supporting information, movie 2).

4. Relating *in situ* sintering studies to operating performance

In favorable cases, *in situ* TEM can provide unique insights into the operation of real-world catalysts. The work of Liu et al. [46] on Pd/alumina catalysts showed that the rapid sintering during catalyst regeneration could be caused by the gasification of carbon leading to agglomeration of the Pd particles. This work helped explain why an otherwise stable Pd/alumina catalyst would sinter so readily during catalyst regeneration. Fortunately, in that study, the time frame for catalyst regeneration in the *in situ* TEM matched that used in the *ex situ* reactor. However, for catalysts which operate in a reactor over long times, sometimes years, how can the insights gained from *in situ* studies be related to the observed phenomena in the real-world operation of industrial catalysts? There is no temperature gap, since one can heat the sample to similar temperatures in current *in situ* cells. However, there is a materials gap (model catalysts), a pressure gap (up to a few mbar in the TEM), and a temporal gap (short time observation in the TEM). Below, some approaches to link the *in situ* observations to the long-term operating performance of supported catalysts are discussed.

The observations made in the initial stages of catalyst sintering for a Ni/$MgAl_2O_4$ indicated that the smallest particles disappear rapidly (in a few seconds) at temperatures in the range 650–750 °C and various gaseous environments (1:1–1:9 H_2:H_2O at 360 Pa). These conditions emulate those of steam reforming, albeit at much lower pressures and the absence of additional carbon which may contribute to particle sintering. Despite the size of particles being small (<5 nm) migration of particles and their coalescence was insignificant compared to Ostwald ripening of the particles. The disappearance of a single Ni nanoparticle was reported recently [64] along with a movie showing time-lapse images of the evolution of the catalyst. The experimentally obtained time trajectory of the decay of an individual nanoparticle, as shown in Fig. 14, could be used to derive a single parameter that captures the energetics of ripening (E_{tot}). The parameter E_{tot} represents the activation barrier for this process of ripening and includes the energy needed to remove the atom from the metal particle and the diffusion barriers on the surface. The smooth curve in this figure represents the calculated time evolution of this Ni particle. The energetic parameter derived from the disappearance of a single nanoparticle was used to explain the evolution of a collection of nanoparticles in this catalyst aged for 30 min with the beam off

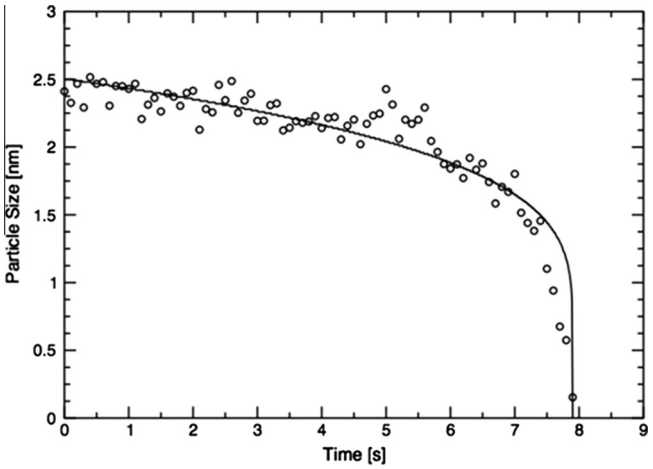

Fig. 14. Size evolution of a 2.5-nm Ni nanoparticle during ripening on $MgAl_2O_4$, experimental (circles) and best-fit predictions based on a mean-field ripening model (adapted from Challa et al. [64]).

[64]. This demonstrates a proof-of-principle that observations at high resolution over short durations can reveal mechanism and rates of the process of sintering that could potentially enable long-duration and large-scale predictions on a realistic catalyst. More work needs to be done to permit such mechanistic studies to make reliable predictions of long-term behavior since local inhomogeneities, support effects, and the role of gas atmosphere need to be fully accounted in the model. For a given catalyst, pretreatment could have a major effect, for example, treating Pt/alumina in oxidizing environments was shown to lead to enhanced stability [67].

Another observable parameter for an industrial catalyst is the loss of surface area (or activity) as a function of time. A manifestation of the different operating mechanisms was believed to appear in the kinetics of decay of surface area of the catalyst. The decay in surface area of supported Ni during operation at elevated temperatures has been studied previously [68–70], and a universal power-law model for the kinetics of surface area loss has been proposed [69]. Of key interest in this model is the exponent "*n*" that is dependent on the dominant mechanism of sintering. Typical values

of "*n*" have been suggested to be between 2–3 for ripening and >5 for migration and coalescence [71]. In previous studies [68–70] of supported Ni particles, this exponent was noted to decrease from a high value to a low value over the duration of sintering. It was therefore suggested that sintering during initial stages (characterized by large exponent "*n*") was dominated by particle migration and coalescence, with later stage sintering occurring via Ostwald ripening. Such a shift in mechanism would be consistent with the expectation that small particles should be more mobile than larger particles, which was clearly not seen at the early stages of heating for the $Ni/MgAl_2O_4$ catalyst. This again stresses the importance of *in situ* observations for individual catalysts, as the predicted mechanism may differ from what actually occurs.

Our *in situ* studies, as well as others reviewed from the literature, suggest that Ostwald ripening can play a major role in the initial evolution of a catalyst. Can the OR model explain the observed trajectory for loss of metal surface area versus time-on-stream? A mechanistic model based on OR was used to calculate the loss in surface area over time using the same energetic parameter (E_{tot}) derived from a fit to the disappearance of individual nanoparticles. As shown in Fig. 15, the early loss of surface area in this catalyst over short time periods is captured. The comparison is reasonable as it is only meant to show the significant loss that occurs during the initial stages of heating. TEM images only show a small region of the sample, and it is not easy to obtain estimates of the surface area of a catalyst based solely on small area TEM images. Additional aspects, such as changes in particle shape with size, add to the uncertainty of the derived surface area at later times. Future work will help us link the observed surface area measured by chemisorption or reactivity measurements to key energetic parameters obtained from *in situ* studies.

Finally, atomistic Monte Carlo (MC) simulation can also be used to predict the evolution of particle size in a model catalyst. Such simulations allow one to relate catalyst sintering to processes taking place at the atomic level, where the random hopping of atoms from site to site is modeled. MC modeling has been applied to a system of nanoparticles (details are presented in Supporting information). Despite employing a simple setup based on the 3D lattice gas model, several characteristic features of sintering of nanoparticles can be seen in these atomistic model systems. Ripening of nanoparticles was the most prevalent mechanism. Also, analyzing the size decay profiles of several disappearing particles clearly showed the Gibbs–Thompson effect on the stability of curved nanoparticles and explains why these particles decay so quickly in the last stages of their disappearance. These calculations validate the underlying mechanistic picture for the rapid disappearance of small particles presented in Figs. 10–12.

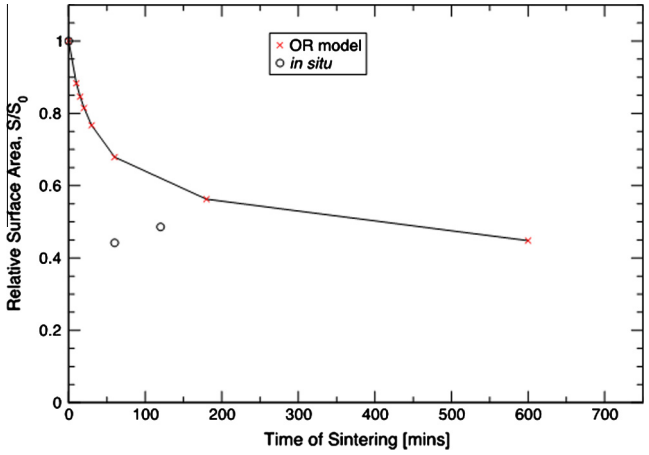

Fig. 15. Decrease in surface area (S/S_0) or relative dispersion (D_0/D) of Ni nanoparticles as estimated from *in situ* images over the course of sintering at 750 °C. The decrease is shown for early stage experiments and for the predictions based on OR modeling.

Fig. 12 presented the ripening behavior of several Ni nanoparticles (shown in Fig. 11) from the *in situ* sintering study. One can notice the slower decay of a small particle (particle 4, 2 nm) compared to other similar size particles. In contrast, a larger particle (particle 1, 2.5–3.0 nm) disappears much faster than this particle. It is clear that local correlations affect the ripening rates of individual nanoparticles; care must be taken when interpreting the E_{tot} values obtained by fitting the decay profiles to simplified ripening models. Further work needs to be done to link these *in situ* observations to the performance of real-world catalysts. The newly developed windowed cells will allow bridging of the pressure gap [32]. As illustrated by the $Ni/MgAl_2O_4$ study that used a powder catalyst prepared just like a conventional supported catalyst, it is possible to gain mechanistic insights also from these complex three dimensional catalyst materials.

5. Summary and conclusions

Current understanding of catalyst sintering is based on two dominant, and distinct, mechanisms of sintering: Ostwald ripening, wherein smaller particles diminish and larger particles grow in size, and particle migration and coalescence, wherein diffusive mobility of particles and ensuing collisions among them causes particle growth [71]. Both mechanisms lead to an overall increase in average particle size and loss of active surface area, but early work suggested that it would be possible to identify the underlying mechanism of sintering based on the shape of particle size distributions and the kinetics of decay in surface area [71,72]. The ability to infer sintering mechanism from size distributions has been questioned [11,73] since the log-normal distribution is the most commonly observed size distribution for heterogeneous catalysts and could likely result from either mechanism [63,72,74,75]. It was also noted that a decay in surface area cannot identify the underlying sintering mechanism as demonstrated in Fig. 12 based on a deterministic model (and in the Supporting information based on a MC simulation). Hence, these decay kinetics are not reliable as a means for deducing mechanisms, and direct observations of catalyst sintering are essential to identify operating mechanisms.

In this work, recent studies on catalyst sintering (over the past decade) that utilized *in situ* electron microscopy have been reviewed. The remarkable improvement in image resolution made possible by the correction of spherical aberrations has made atomically resolved images routinely obtainable. Tables 1 and 2 summarized the recent studies of catalyst sintering via *in situ* EM. Table 1 includes those studies where the authors concluded that particle migration and coalescence was the dominant mechanism for their system. Several of these studies used the electron beam as the sole source of heating and several of those were on carbon substrates. It is well known that carbon suffers from knock-on damage when imaged with 200–300 kV electrons, and carbon can be gasified by reaction with H_2 or with O_2 that can lead to enhanced mobility of nanoparticles. In this context, the important effect reported by Batson et al.[48] needs to be considered. They showed that electron beam illumination could induce forces among particles, which could lead to coalescence. Therefore, to obtain insights relevant to heterogeneous catalysis, we should focus our attention on studies where the sample had to be heated to observe sintering (as is generally the case in heterogeneous catalysts). There are several studies in Tables 1 and 2 that used ETEM to study catalysts that were heated in the presence of a gas. Among these, the majority of studies report that Ostwald ripening is the primary operative mechanism; but, there are also reports of particle migration and coalescence, as inferred through continuous direct observation

via *in situ* TEM. However, it is important to note that the reports of nanoparticle mobility do not follow the expectation of Brownian-like motion or the expectation that the smallest particles would be the most mobile.

The work described on $Ni/MgAl_2O_4$ provides direct high-resolution *in situ* observations of Ni particle growth in a powder catalyst very similar to industrial Ni catalysts used for steam reforming of methane. In the initial stages when the $Ni/MgAl_2O_4$ reaches the operating temperature, very fast ripening of the smallest Ni particles is observed. Since these smallest nanoparticles contribute significantly to the total surface area, one observes a very rapid drop in surface area in the initial stages when these small particles disappear. Monte Carlo simulations showed that the observed phenomena could be recreated based on a physical model that only permitted atom mobility. The MC simulations confirmed the particle size evolution in the early stages of sintering with rapid loss of small particles and negligible particle mobility. The nature of the mobile species that cause ripening could not be deduced from these experiments. As suggested in previous work by Sehested [75], it is entirely likely that the interaction of surface hydroxyls on Ni may result in a mobile species that mediates sintering. This is a better explanation than vapor-phase emission of Ni atoms (evaporation), since the rate of ripening of the small Ni particle far exceeds the rate at which this particle would evaporate in vacuum at the operating temperature [64,76].

Our observations on $Ni/MgAl_2O_4$ showed particle migration and coalescence most clearly at later stages of sintering, when the smallest particles had disappeared due to Ostwald ripening. An important parameter that has not been adequately considered in this context is the interparticle separation, which can also influence catalyst sintering [77]. This is generally difficult to quantify in a three dimensional support, but recently, it was shown by using electron tomography [78] that interparticle separations could be measured and found to play an important role. Samples which were located in close proximity were more susceptible to sinter via migration and coalescence. Therefore, we conclude that both ripening and particle migration and coalescence can contribute to the observed rates of catalyst sintering during the industrial operation of these catalysts. The relative contribution of these two mechanisms to the observed rates of sintering has not yet been conclusively established and will be the subject of future studies. We also point out that most *in situ* studies of catalyst sintering are performed under conditions of pressure and temperature far removed from industrial practice. However, that has changed with the development of new MEMS based sample holders that allow heating to temperatures of up to 1000 °C under oxidizing conditions and with windows, and it is also possible to perform *in situ* studies at atmospheric pressure [32]. However, most *in situ* observations are performed over short times; so, we suggest that, by using mechanistic models, it is possible to derive key energetic parameters from these short term observations to make predictions of the longer term performance of industrial catalysts. In summary, we can state that *in situ* TEM has provided unique insights on catalyst sintering and recent instrumental developments will further accelerate progress in the area to prevent catalyst sintering and in catalyst engineering.

Acknowledgments

The authors would like to dedicate this review to Dr. Haldor Topsøe who recently passed away in 2013, just a few days shy of his 100th birthday. His vision and leadership led to the establishment of the high-resolution *in situ* electron microscopy facilities at the Topsøe laboratories in Denmark. The authors thank him and his coworkers for hosting one of us (AD) on a sabbatical visit and for providing two PhD students (ADLR and TWH) an opportunity to complete part of their PhD research using these *in situ* microscopy facilities. We acknowledge financial support from the following Grants: NSF GOALI CBET-1067803, NSF IGERT DGE-0504276, and NSF PIRE OISE-0730277, Partnership for International Research and Education.

Appendix A. Supplementary data

Supplementary data associated with this article can be found, in the online version, at http://dx.doi.org/10.1016/j.jcat.2013.08.018.

References

[1] M. Knoll, E. Ruska, Z. Angew. Phys. 78 (1932) 318–339.
[2] M. Behrens, F. Studt, I. Kasatkin, S. Kühl, M. Hävecker, F. Abild-Pedersen, S. Zander, F. Girgsdies, P. Kurr, B.L. Kniep, M. Tovar, R.W. Fischer, J.K. Nørskov, R. Schlögl, Science 336 (2012) 893–897.
[3] T.W. Hansen, J.B. Wagner, P.L. Hansen, S. Dahl, H. Topsoe, C.J.H. Jacobsen, Science 294 (2001) 1508–1510.
[4] C.J.H. Jacobsen, S. Dahl, P.L. Hansen, E. Tornqvist, L. Jensen, H. Topsoe, D.V. Prip, P.B. Moenshaug, I. Chorkendorff, J. Mol. Catal. A-Chem. 163 (2000) 19–26.
[5] M.D. Shroff, D.S. Kalakkad, K.E. Coulter, S.D. Koehler, M.S. Harrington, N.B. Jackson, A.G. Sault, A.K. Datye, J. Catal. 156 (1995) 185–207.
[6] H.N. Pham, L. Nowicki, J. Xu, A.K. Datye, D.B. Bukur, C. Bartholomew, Ind. Eng. Chem. Res. 20 (2003) 4001–4008.
[7] J.J.F. Scholten, A. van Montfoort, J. Catal. 1 (1962) 85–92.
[8] J.C. Yang, M.W. Small, R.V. Grieshaber, R.G. Nuzzo, Chem. Soc. Rev. 41 (2012) 8179–8194.
[9] A.K. Datye, J. Catal. 216 (2003) 144–154.
[10] D.S. Su, ChemCatChem 3 (2011) 919–920.
[11] P.L. Hansen, S. Helveg, A.K. Datye, Adv. Catal. 50 (2006) 77–95.
[12] A. DeLaRiva, Sintering of Ni/MgAl2O4 catalyst via in-situ TEM, in: Chemical and Nuclear Engineering. University of New Mexico, Albuquerque, NM, USA, 2010.
[13] F.S. Feates, Chem Ind August (1970) 1103–1104.
[14] R.T.K. Baker, Catal. Rev.-Sci. Eng. 19 (1979) 161.
[15] E.D. Boyes, P.L. Gai, Ultramicroscopy 67 (1997) 219–232.
[16] P.L. Gai, Top. Catal. 8 (1999) 97–113.
[17] M. von Ardenne, Z. Angew. Phys. 109 (1938) 553–572.
[18] F. Krause, Naturwissenschaften 25 (1937) 817–825.
[19] E. Ruska, Kolloid-Z 100 (1942) 212–219.
[20] P.R. Swann, N.J. Tighe, JernKont. Ann. 155 (1971).
[21] H. Hashimoto, T. Naiki, Jpn. J. Appl. Phys. 7 (1968) 946–952.
[22] R.T.K. Baker, P.S. Harris, J. Phys. E-Sci. Instrum. 5 (1972) 793.
[23] P.L. Gai, E.D. Boyes, S. Helveg, P.L. Hansen, S. Giorgio, C.R. Henry, MRS Bull. 32 (2007) 1044–1050.
[24] S. Helveg, C. Lopez-Cartes, J. Sehested, P.L. Hansen, B.S. Clausen, J.R. Rostrup-Nielsen, F. Abild-Pedersen, J.K. Norskov, Nature 427 (2004) 426–429.
[25] P.L. Hansen, J.B. Wagner, S. Helveg, J.R. Rostrup-Nielsen, B.S. Clausen, H. Topsøe, Science 295 (2002) 2053–2055.
[26] R. Sharma, P.A. Crozier, in: E.N. Yao, Z.L. Wang (Eds.), Handbook of Microscopy for Nanotechnology, Springer, 2005.
[27] T.W. Hansen, J.B. Wagner, R.E. Dunin-Borkowski, Mater. Sci. Technol. 26 (2010) 1338–1344.
[28] J.B. Wagner, F. Cavalca, C.D. Damsgaard, L.D.L. Duchstein, T.W. Hansen, Micron 43 (2012) 1169–1175. Oxford, England: 1993.
[29] T.W. Hansen, J.B. Wagner, Microsc. Microanal. 18 (2012) 684–690.
[30] H. Yoshida, Y. Kuwauchi, J.R. Jinschek, K.J. Sun, S. Tanaka, M. Kohyama, S. Shimada, M. Haruta, S. Takeda, Science 335 (2012) 317–319.
[31] T. Kamino, T. Yaguchi, M. Konno, A. Watabe, T. Marukawa, T. Mima, K. Kuroda, H. Saka, S. Arai, H. Makino, Y. Suzuki, K. Kishita, J. Electron Microsc. 54 (2005) 497–503.
[32] L.F. Allard, S.H. Overbury, W.C. Bigelow, M.B. Katz, D.P. Nackashi, J. Damiano, Microsc. Microanal. 18 (2012) 656–666.
[33] J.F. Creemer, S. Helveg, G.H. Hoveling, S. Ullmann, A.M. Molenbroek, P.M. Sarro, H.W. Zandbergen, Ultramicroscopy 108 (2008) 993–998.
[34] T. Alan, T. Yokosawa, J. Gaspar, G. Pandraud, O. Paul, F. Creemer, P.M. Sarro, H.W. Zandbergen, Appl. Phys. Lett. 100 (2012).
[35] J.R. Jinschek, S. Helveg, Micron 43 (2012) 1156–1168.
[36] L.F. Allard, W.C. Bigelow, M. Jose-Yacaman, D.P. Nackashi, J. Damiano, S.E. Mick, Microsc. Res. Tech. 72 (2009) 208–215.
[37] J.F. Creemer, W. Van der Vlist, C.R.D. Boer, H.W. Zandbergen, P.M. Sarro, D. Briand, N.F. De Rooij, IEEE Sensors 1 and 2 (2005) 330–333.
[38] R.T.K. Baker, F.S. Feates, P.S. Harris, Carbon 10 (1972) 93–96.
[39] R.T.K. Baker, C. Thomas, R.B. Thomas, J. Catal. 38 (1975) 510–513.
[40] R.T.K. Baker, P.S. Harris, R.B. Thomas, Surf. Sci. 46 (1974) 311–316.
[41] H. Chen, Y. Yu, H.L. Xin, K.A. Newton, M.E. Holtz, D. Wang, D.A. Muller, H.D. Abruña, F.J. DiSalvo, Chem. Mater. (2013).
[42] K. Yoshida, X. Zhang, A.N. Bright, K. Saitoh, N. Tanaka, Nanotechnology 24 (2013) 065705.
[43] I. Janowska, M.S. Moldovan, O. Ersen, H. Bulou, K. Chizari, M.J. Ledoux, P.H. Cuong, Nano Res. 4 (2011) 511–521.

[44] C. Aydin, J. Lu, N.D. Browning, B.C. Gates, Angew. Chem.-Int. Ed. 51 (2012) 5929–5934.
[45] H. Hirata, K. Kishita, Y. Nagai, K. Dohmae, H. Shinjoh, S. Matsumoto, Catal. Today 164 (2011) 467–473.
[46] R.-J. Liu, P.A. Crozier, C.M. Smith, D.A. Hucul, J. Blackson, G. Salaita, Microsc. Microanal. 10 (2004) 77–85.
[47] E. Ruckenstein, S.H. Lee, J. Catal. 86 (1984) 457–464.
[48] P.E. Batson, A. Reyes-Coronado, R.G. Barrera, A. Rivacoba, P.M. Echenique, J. Aizpurua, Nano Lett. 11 (2011) 3388–3393.
[49] P.E. Batson, A. Reyes-Coronado, R.G. Barrera, A. Rivacoba, P.M. Echenique, J. Aizpurua, Ultramicroscopy 123 (2012) 50–58.
[50] A.D. Benavidez, L. Kovarik, A. Genc, N. Agrawal, E.M. Larsson, T.W. Hansen, A.M. Karim, A.K. Datye, ACS Catal. 2 (2012) 2349–2356.
[51] W.C. Yang, M. Zeman, H. Ade, R.J. Nemanich, Phys. Rev. Lett. 90 (2003) 136102.
[52] K. Yoshida, A. Bright, N. Tanaka, J. Electron Microsc. 61 (2012) 99–103.
[53] F.M. Ross, Rep. Prog. Phys. 73 (2010).
[54] J.B. Hannon, S. Kodambaka, F.M. Ross, R.M. Tromp, Nature 440 (2006) 69–71.
[55] S. Kodambaka, J.B. Hannon, R.M. Tromp, F.M. Ross, Nano Lett. 6 (2006) 1292–1296.
[56] P.B. Amama, C.L. Pint, S.M. Kim, L. McJilton, K.G. Eyink, E.A. Stach, R.H. Hauge, B. Maruyama, ACS Nano 4 (2010) 895–904.
[57] P.B. Amama, C.L. Pint, L. McJilton, S.M. Kim, E.A. Stach, P.T. Murray, R.H. Hauge, B. Maruyama, Nano Lett. 9 (2009) 44–49.
[58] S.M. Kim, C.L. Pint, P.B. Amama, R.H. Hauge, B. Maruyama, E.A. Stach, J. Mater. Res. 25 (2010) 1875–1885.
[59] S.M. Kim, C.L. Pint, P.B. Amama, D.N. Zakharov, R.H. Hauge, B. Maruyama, E.A. Stach, J. Phys. Chem. Lett. 1 (2010) 918–922.
[60] D.N. Futaba, K. Hata, T. Yamada, K. Mizuno, M. Yumura, S. Iijima, Phys. Rev. Lett. 95 (2005) 056104.
[61] K. Hata, D.N. Futaba, K. Mizuno, T. Namai, M. Yumura, S. Iijima, Science 306 (2004) 1362–1364.
[62] M.A. Brown, Y. Fujimori, F. Ringleb, X. Shao, F. Stavale, N. Nilius, M. Sterrer, H.J. Freund, J. Am. Chem. Soc. 133 (2011) 10668–10676.
[63] T.W. Hansen, Sintering and particle dynamics in supported metal catalysts, in: Department of Chemistry, Technical University of Denmark, Lyngby, 2006.
[64] S.R. Challa, A.T. Delariva, T.W. Hansen, S. Helveg, J. Sehested, P.L. Hansen, F. Garzon, A.K. Datye, J. Am. Chem. Soc. 133 (2011) 20672–20675.
[65] S.B. Simonsen, I. Chorkendorff, S. Dahl, M. Skoglundh, J. Sehested, S. Helveg, J. Am. Chem. Soc. 132 (2010) 7968–7975.
[66] B. Schaffer, W. Grogger, G. Kothleitner, Ultramicroscopy 102 (2004) 27–36.
[67] J. Matos, L.K. Ono, F. Behafarid, J.R. Croy, S. Mostafa, A.T. DeLaRiva, A.K. Datye, A.I. Frenkel, B.R. Cuenya, Phys. Chem. Chem. Phys. 14 (2012) 11457–11467.
[68] C.H. Bartholomew, W.L. Sorensen, J. Catal. 81 (1983) 131–141.
[69] J.T. Richardson, J.G. Crump, J. Catal. 57 (1979) 417–425.
[70] J. Sehested, J. Catal. 217 (2003) 417–426.
[71] P. Wynblatt, N.A. Gjostein, Prog. Solid State Chem. 9 (1975) 21.
[72] C.G. Granqvist, R.A. Buhrman, J. Catal. 42 (1976) 477.
[73] G.A. Fuentes, E.D. Gamas, Stud. Surf. Sci. Catal. 68 (1991) 637.
[74] G.A. Fuentes, E. Salinas-Rodriguez, Stud. Surf. Sci. Catal. 139 (2001) 503.
[75] J. Sehested, J.A.P. Gelten, S. Helveg, Appl. Catal. A-General 309 (2006) 237–246.
[76] H.A. Jones, I. Langmuir, M.J. Mackay, Phys. Rev. 30 (1927) 201–214.
[77] L.K. Ono, B. Roldan-Cuenya, Catal. Lett. 113 (2007) 86–94.
[78] G. Prieto, J. Zecevic, H. Friedrich, K.P. de Jong, P.E. de Jongh, Nat. Mater. 12 (2013) 34–39.